Improving pulsed laser weldability of duplex stainless steel to 5456 aluminum alloy via friction stir process reinforcing of aluminum by BNi-2 brazing alloy

Hossein ESMAILY, Ali HABIBOLAHZADEH, Mohammad TAJALLY

Faculty of Materials and Metallurgical Engineering, Semnan University, Semnan 35351-19111, Iran

Abstract: Effects of laser pulse distance and reinforcing of 5456 aluminum alloy were investigated on laser weldability of Al alloy to duplex stainless steel (DSS) plates. The aluminum alloy plate was reinforced by nickel-base BNi-2 brazing powder via friction stir processing. The DSS plates were laser welded to the Al5456/BNi-2 composite and also to the Al5456 alloy plates. The welding zones were studied by scanning electron microscopy, X-ray diffractometry, micro-hardness and shear tests. The weld interface layer became thinner from 23 to 5 μm, as the laser pulse distance was increased from 0.2 to 0.5 mm. Reinforcing of the Al alloy modified the phases at interface layer from Al−Fe intermetallic compounds (IMCs) in the DSS/Al alloy weld, to Al−Ni−Fe IMCs in the DSS/Al composite one, since more nickel was injected in the weld pool by BNi-2 reinforcements. This led to a remarkable reduction in crack tendency of the welds and decreased the hardness of the interface layer from ~950 HV to ~600 HV. Shear strengths of the DSS/Al composite welds were significantly increased by ~150%, from 46 to 114 MPa, in comparison to the DSS/Al alloy ones.

Key words: duplex stainless steel (DSS); Al5456 aluminum alloy; BNi-2 brazing alloy; friction stir processing; pulsed laser welding

1 Introduction

The most objection in the welding of steel to aluminum is the formation of a brittle intermetallic layer at the interface [1]. Controlling the intermetallic compounds (IMC) formation is the main key in improving the weldability and strength of steel/aluminum [2,3].

The welding of the steel to aluminum has been performed by laser beam welding (LBW) technique, which provided highly-concentrated low heat input [4]. The quality of LBW was further improved by employing supplementary techniques, such as using pulse mode in laser welding [5], and steel as top-side at lap joint [6]. However, large amounts of brittle Fe−Al IMC were still formed at the interface of fusion zone (FZ) with base metals (BM). Hence, investigations were conducted to properly modify the chemical composition of the steel/aluminum interface layer. In this respect, zinc [7,8], silicon [9] or nickel [10] was injected to the interface layer to make proper chemical change. Using a nickel foil at the interface showed no defect or any limitation accompanied by zinc and silicon additions [11,12]. Nickel moderately softened and modified the very hard and brittle Fe−Al IMC at the interface of the steel/aluminum weldment; however, the substituted Fe−Al−Ni IMC was not highly ductile as Fe−Al−Zn or Fe−Al−Si IMC [10,13].

Recently, new solid-state methods are developed which can produce metal/metal composite. Among them, friction stir processing (FSP) is a promising method which can reinforce Al alloy with nickel or nickel-base alloy, without matrix/particle reaction [14,15]. During welding to duplex stainless steel (DSS), the Al alloy/Ni-base alloy particle composite can feed Ni in the fusion zone or at the FZ/BM interface.

In the present study, it was attempted to improve the pulsed laser weldability of 1.4362 duplex stainless steel to 5456 aluminum alloy, through pre-reinforcing of the aluminum alloy surface. The surface of the aluminum was initially reinforced by the powder of the BNi-2 brazing alloy, via friction stir processing (FSP). The reinforcing powder is nickel-base and also contains some silicon. The reports indicated that the nickel-base BNi-2 alloy had a good joinability to steels [16]. In addition, its

melting temperature is considerably lower than that of the pure nickel, so, lower heat input is needed to remelt BNi-2 particle than that of pure nickel. It could be expected that the presence of BNi-2 reinforcements injects nickel and silicon into the DSS/Al5456 interface. They reduce the amounts of brittle Fe−Al IMCs at the interface, and may change them to the more ductile ones in Fe−Al−Ni system. The investigating of weldability of DSS to the Al5456/BNi-2 brazing alloy is reported for the first time here and the results have been discussed.

2 Experimental

Al5456 aluminum alloy plate was reinforced by BNi-2 powder via friction stir processing (FSP). Typical alloying elements are shown in Table 1. A straight groove with a square cross-section of 2 mm × 2 mm was machined on the aluminum plate and filled by BNi-2 powder (Nicrobraz LM) with the particle size of <44 μm. A rotating tool from hardened H13 tool steel was selected for FSP, having a shoulder and a threaded pin with diameters of 14 and 3.4 mm, respectively, and height of 2.7 mm. The threads had 0.6 mm spacing and tool tilt angle was 2°. The tool rotated clockwise at speed of 1250 r/min and advanced with traveling speed of 10 mm/min. Macrograph of FSP cross sections (three transverse cross sections) shows that the stir zone contains ~9 vol.% BNi-2 particles (white spots) and has ~1.9 mm height, with almost uniformly distributed reinforcements (Fig. 1). Plates of 1.4362 duplex stainless steel (DSS) with 80 mm × 20 mm × 0.5 mm, and Al5456/BNi-2 aluminum composite with 80 mm × 20 mm × 5 mm dimensions were cut for laser beam welding (Fig. 2).

A Nd:YAG laser (Vision LWI V T-BaseV3) with a maximum power of 120 W was used for laser welding (Fig. 2). Laser energy, traveling speed, beam diameter,

and pulse duration was 61.4 J, 0.2 mm/s, 1.4 mm and 0.02 s, respectively. Pulse distances (intervals between two consecutive pulses) were selected as 0.2, 0.3, 0.4 and 0.5 mm (Table 2). The power density of laser (ratio of power to laser spot area) was calculated as 1994 W/mm^2. Two series of samples were prepared for pulsed laser welding; (1) DSS/Al5456 alloy (Alx samples) and (2) DSS/BNi-2−5456 Al alloy composite (Cx samples), as seen in Table 2 and Fig. 2.

The aluminum (alloy or composite) as the lower plate, and DSS as the top plate were fastened to each other by a fixture during welding. Before welding, the surfaces of the DSS, the aluminum alloy and the aluminum composite were polished. For each parameter in Table 2, four coupons were welded according to the lap weld clause of ISO15614−11:2002, with dimensions as mentioned above. Three of as-welded samples were used for the tensile shear tests according to AWS B4.0:2016, with a test fixture according to AWS C3.2:2008, without any additional preparation. The average value was reported. The velocity of the grips during the shear test was 3 mm/min. The forth coupon was utilized for microstructure analysis and the temperature measurement.

DSS/aluminum alloy and DSS/aluminum composite weldments are designated by Alx and Cx, respectively, where x stands for pulse distances (intervals between two consecutive pulses) of 0.2, 0.3, 0.4 or 0.5 mm. Temperatures of samples were recorded during welding by inserting a thermocouple inside a hole with 12 mm in distance from the weld centerline (Fig. 2). Maximum temperature was considered for later comparison.

Microstructures of the weldments were studied by scanning electron microscope (SEM, TESCAN MIRA3) coupled by an energy dispersive X-ray spectroscope (EDS). X-ray diffractometery (XRD) was obtained by Bruker (D8 advance) instrument, using Cu K$_\alpha$ radiation

Table 1 Chemical compositions of alloys of 1.4362 DSS, Al5456 and BNi−2 (wt.%)

Material	Fe	Cr	Ni	C	N	Mo	B	Si	Al	Mg	Mn
1.4362 DSS	Bal.	21.8	4.1	0.03	0.11	0.46	−	0.68	−	−	1.82
Al5456	−	−	−	−	−	−	−	−	Bal.	5.3	0.5
BNi−2	3.01	7.1	Bal.	−	−	−	3.12	4.5	−	−	−
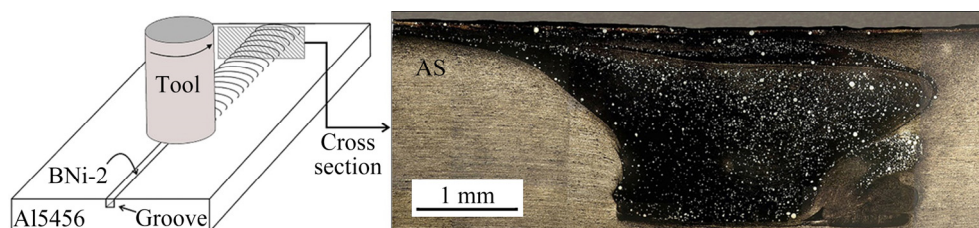
Fig. 1 Schematic illustration of FSP process and cross sectional macrostructure of stir zone in FSP composite (AS is advancing side of stir zone)
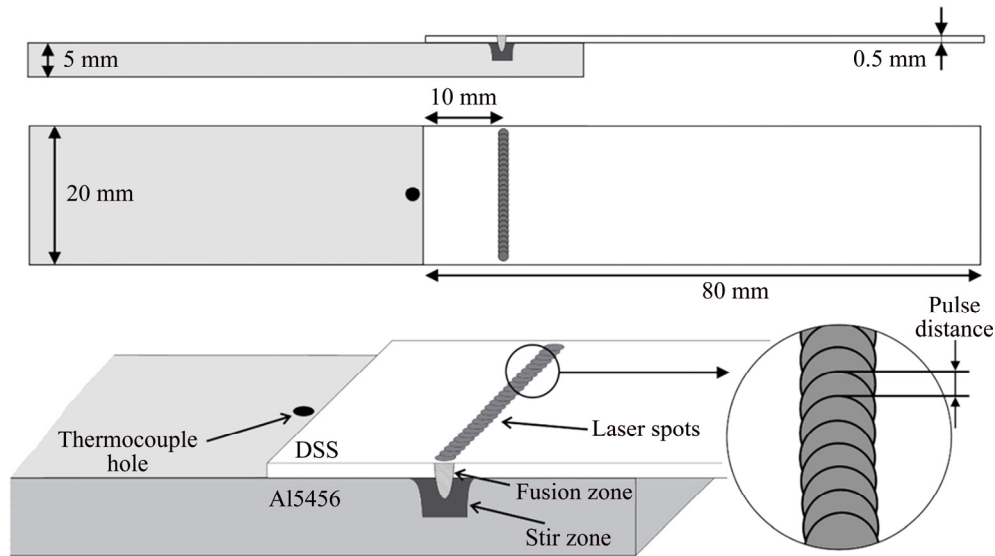
Fig. 2 Laser welding set-up (stir zone exists only in C*x* samples) and size of tensile shear test coupon

Table 2 Summary of samples conditions

| Sample	Pulse distance/mm				Substrate	
	0.2	0.3	0.4	0.5	Al5456	Aluminum composite
Al0.2	✔				✔	
Al0.3		✔			✔	
Al0.4			✔		✔	
Al0.5				✔	✔	
C0.2	✔					✔
C0.3		✔				✔
C0.4			✔			✔
C0.5				✔		✔

with λ=1.54 Å. Microstructural features, such as the thickness of the interface layer, were measured via image analyzing using ImageJ software. Interface layer thickness was measured at minimum 15 points on the fusion zone and the average value was reported. Vickers microhardness (Buehler micromet II) of the fusion zone at centerline was evaluated with about 0.07 mm intervals, using 50 g force and 10 s dwell time. Cracks were avoided from microhardness measurement. Each hardness result was the average of the three measurements around the intervals (0.07 mm) based on ISO 22826:2005.

3 Results and discussion

3.1 Maximum temperature near fusion zone

Maximum temperatures during welding of the different samples are shown in Fig. 3. It is evident that any increase in the laser pulse distance leads to a decrease in the maximum recorded temperature. The reason would be hitting fewer laser pulses in a given length, as pulse intervals become longer, i.e. laser heat input decreases at longer pulse distances.
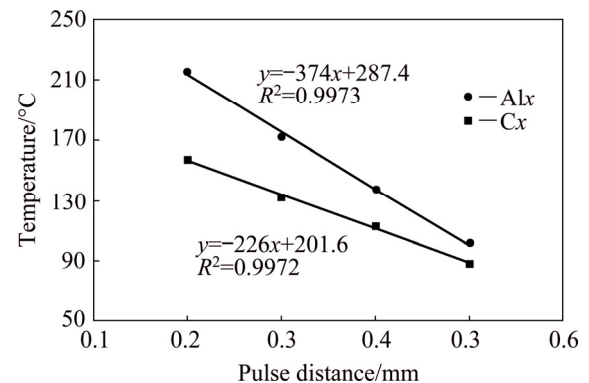

Fig. 3 Maximum temperature at 12 mm in distance from weld centerline, versus pulse distance during welding of Al*x* and C*x* samples

The heat balance at the weld pool can be shown as follows:

$$q_{\text{Laser}}+q_{\text{Reaction}}=q_{\text{Steel melting}}+q_{\text{Al melting}}+q_{\text{Losses}} \tag{1}$$

According to the equation, some of laser heat input (q_{Laser}) causes the melting of DSS ($q_{\text{Steel melting}}$) and aluminum ($q_{\text{Al melting}}$) and some of it losses (q_{Losses}) due to heat conduction, radiation and convection. However, some heat is generated within the weld pool via the exothermic reactions of Al with Fe, Ni and Cr (q_{Reaction}) [17−20]. Such reactions are as follows:

$$a\text{Al}+b\text{Fe(Cr,Ni)} \rightarrow c\text{Al}_x\text{Fe(Cr,Ni)}_y+q_{\text{reaction}} \tag{2}$$
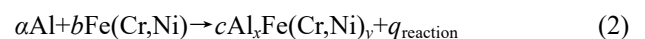
The amount of generated heat by the reaction is proportional to the amount of reacted Al, Fe, Cr and Ni.

The increase of the weld pool height would lead to the increase of aluminum content of the weld pool (as will be discussed in Section 3.3). This results in more aluminides formation and higher $q_{Reaction}$. By changing the aluminum base metal from alloy to composite one, equation for heat balance becomes

$$q_{Laser}+q_{Reaction}=q_{Steel\ melting}+q_{Al\ melting}+q_{BNi\text{-}2\ melting}+q_{Losses} \quad (3)$$

Melting of BNi-2 particles takes more energy rather than aluminum, in a given volume. For instance, the ratio of the required energy for melting and heating up of BNi-2 particles and Al alloy to 1000 °C could be calculated as follows:

$$\frac{q_{BNi\text{-}2}}{q_{Al5456}}=\left[\rho_{BNi\text{-}2}V_{BNi\text{-}2}\left(\int_{298}^{1273}c_p^{BNi\text{-}2}dT+L_f^{BNi\text{-}2}\right)\right]/$$
$$\left[\rho_{BNi\text{-}2}V_{BNi\text{-}2}\left(\int_{298}^{913}c_p^{Al\ solid}dT+L_f^{Al}+\int_{913}^{1273}c_p^{Al\ solid}dT\right)\right]\approx 2$$
$$(4)$$

As will be discussed in Section 3.2, the height of weld pool in Cx samples is shallower than that of Alx ones. Therefore, less heat generation from aluminide-making reactions is anticipated in the Cx samples. It can be considered that the maximum temperature depends on the type of aluminum base metal (alloy or composite), laser heat input and the height of the weld pool (a criterion for the amount of base metals reaction). The relationship is depicted in Fig. 4. The heat input is normalized by dividing to 0.5 mm pulse distance heat input.
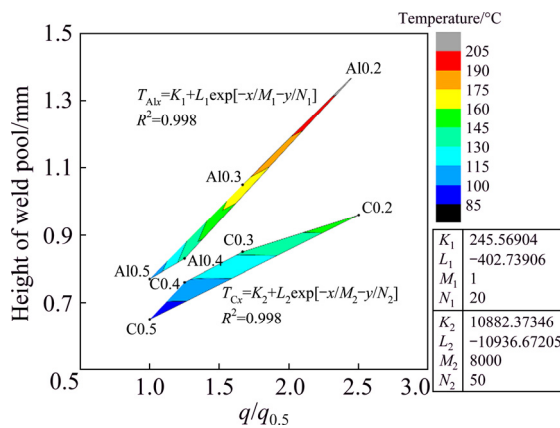
Fig. 4 Temperature versus normalized heat input and height of weld pool (The color legend shows temperature; the fitting constants are shown in the side tables)

Thermal diffusivities are also important, which measure the rate of heat transfer of materials from the hot region to the cold side. Thermal diffusivity is equal to $k/(\rho\times c_p)$, where k, ρ and c_p are thermal conductivity, density and specific heat capacity, respectively. It is 44 mm^2/s for 5456 aluminum alloy [21]. Thermal diffusivity of BNi-2/Al5456 composite is needed to be estimated. In this respect, the thermal conductivity of the

composite was calculated via Lewis−Nielsen model (the thermal conductivity of BNi-2 is 14.65 W/(m·K) and that of Al5456 alloy is 120 W/(m·K)) [22,23], and density and heat capacity were approximated by the rule of mixtures [24]. Eventually, the value of 0.34 mm^2/s was obtained for thermal diffusivity of BNi-2/Al5456 composite, which is much lower than that of aluminum alloy. This means that the laser heat can diffuse much lower in the Cx samples, which results in a shallower weld pool in these samples.

Therefore, during welding, the laser heat is mainly accumulated at the surface layer of the aluminum composite (Cx). Also, BNi-2 particles, which exist only in Cx samples, take more heat during melting. In addition, because of shallower weld pool height, $q_{Reaction}$ is less in Cx samples. Hence, it is expected that the weld pools of Cx samples are cooler.

### 3.2 Macrostructure and fusion zone configuration

Backscattered electron (BSE) SEM micrographs of the fusion zones for eight samples are illustrated in Fig. 5. All Alx, C0.2 and C0.3 samples show micro-crack(s) at their fusion zones or interface regions (white arrows in Fig. 5). Macro-cracks at the interface layer in Al0.2 and Al0.3 samples propagated transversely through the weld zone. The micro-cracks have mainly grown along the weld zone contour. Micro-cracking of Cx samples (instead of macro-crack of Al0.2 and Al0.3 samples) indicates that the amounts of thermally-induced stresses, are smaller in the Cx samples [5]. The reason could be lower temperature of the weld pool in Cx samples during laser welding (Fig. 3 and Section 3.1). Large difference in thermal expansion coefficients of 1.4362 DSS (17.3×10^{-6} K^{-1}), 5456 Al alloy (24×10^{-6} K^{-1}) and the Al$_3$Fe IMC (14.6×10^{-6} K^{-1} [25]) is another important source of cracking during the welding [26].

The thickness of the interface layer versus pulse interval was measured and depicted in Fig. 6. The interface layer is featured by its light grey color, in contrast to white (top DSS) and dark grey (bottom aluminum) colors. Some "dark bands" appear at the inner parts of the fusion zone (black arrows in Fig. 5) in the samples with pulse distances of 0.2 and 0.3 mm. These bands almost have the same color tune as the interface layer has, and have aligned parallel to the fusion zone contour.

Figures 3 and 6 show that the increase in pulse distance reduces the maximum temperature and leads to a thinner interface layer and a shallower weld pool. The thickness and height trends decline more steeply in Alx samples rather than those in Cx samples, which is almost similar to the trends in Fig. 3. The thickness of the interface layer in Cx samples is 60%−80% thinner than in Alx samples. The presence of BNi-2 particles in Cx
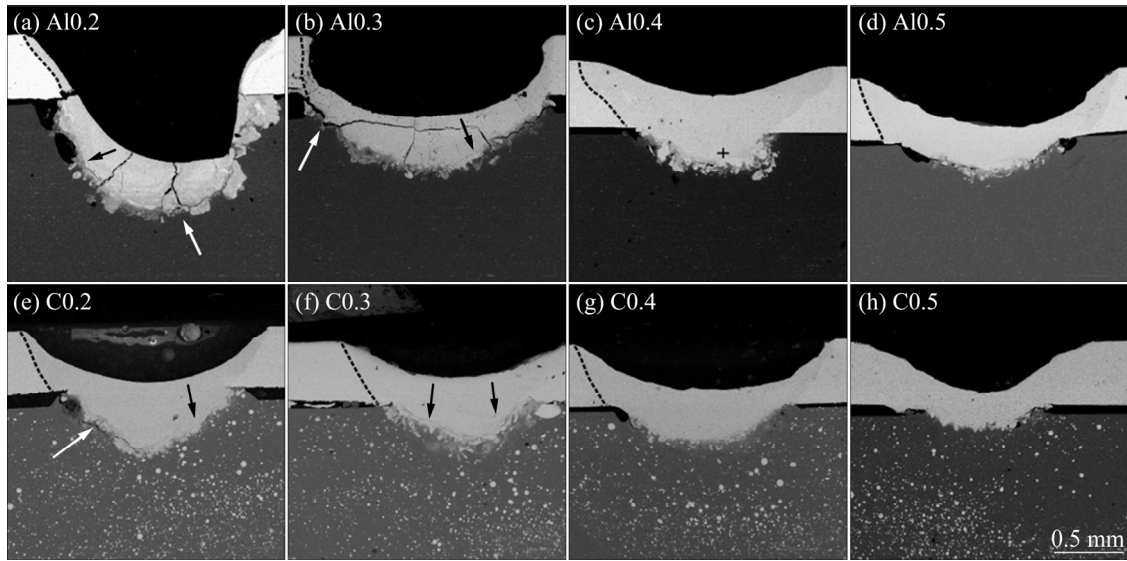
Fig. 5 BSE−SEM macrostructures of samples (White arrows point micro-cracks, black arrows show dark bands, chemical composition of black cursor in Al0.4 is shown in Table 2, and dashed lines show left border of fusion zone with DSS)
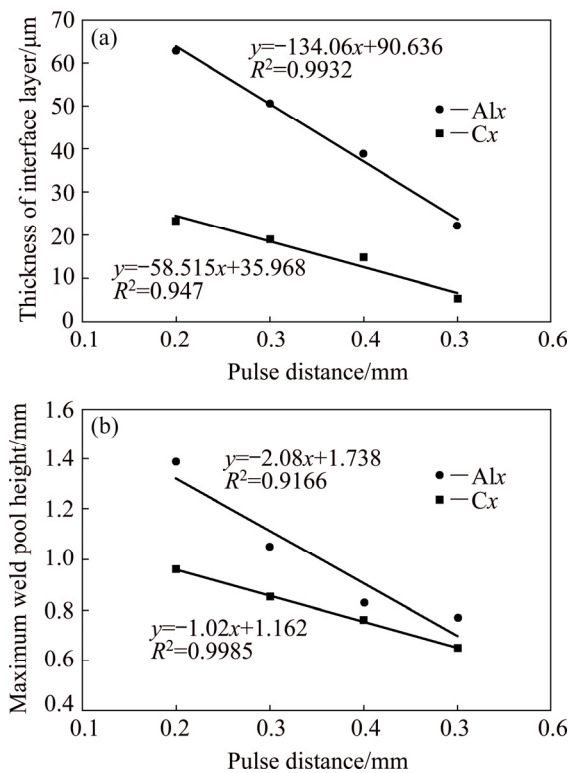
Fig. 6 Thickness of interface layer (a) and maximum weld pool height (b) versus pulse distance in Alx and Cx samples

samples provides new types of IMC formation reactions (as will be discussed in Section 3.4), and also, they absorb higher heat energy to heat up (Eq. (1)). Therefore, it changes the intermetallic type(s) and decreases the volume of the weld pool and its volume of sinking and undercut. Also, the Cx samples have experienced lower temperature, and less amount of interactions at the interface is expected, which is in contrast to the Alx samples.

The observed dark bands in the fusion zone apparently have the same origin as "banded structure", according to CHEN et al [10], or "solute band" according to SIERRA et al [6]. Based on their work, the formation of the bands could be the consequence of convection flow in the weld pool. During the welding process, initially, top side DSS melts; later, the aluminum beneath the DSS starts to melt and the high-density liquid DSS flows downward, mixes and interacts with the liquid aluminum; subsequently, the low-density product (which shows itself by dark bands in BSE−SEM images) moves upward due to the convection flow in the weld pool [6,10,27]. Since molten pool has the lower temperature in the samples with the pulse distances of 0.4 and 0.5 mm (Fig. 3), the convection flow is almost ceased and no dark bands are observed in the samples with over 0.3 mm pulse distances (Fig. 5).

3.3 Chemical composition of fusion zone

The SEM line scan analysis results of the samples C0.5, C0.2 and Al0.2 are shown in Fig. 7. The interface zone is assigned by a dashed square. The border of the interface layer in C0.5 is distinct and sharp. However, the interface zone of the samples C0.2 and Al0.2 cannot be easily distinguished, because of heavy interactions between base metals. Comparing aluminum content of C0.2 and C0.5 reveals that the low amount of aluminum is diffused into the fusion zone of C0.5 and Al5456/DSS reactions are constrained to the interface zone. Meanwhile, the amount of aluminum reaches about 15 wt.% at the surface of the fusion zone of C0.2. Since
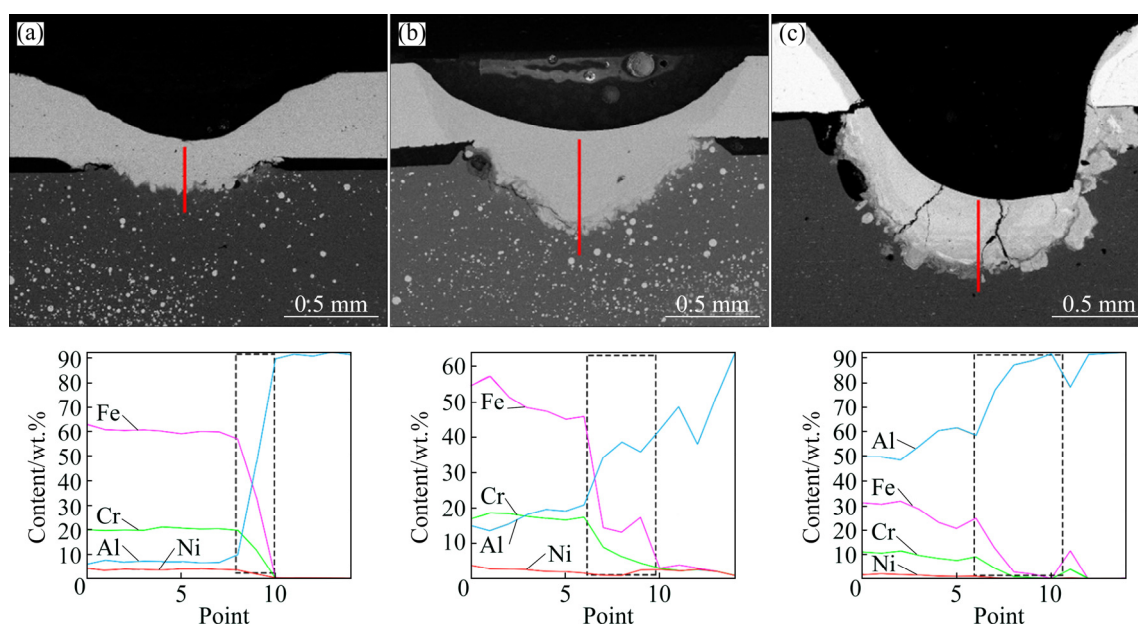
Fig. 7 EDS line scans of C0.5 (a), C0.2 (b) and Al0.2 (c) samples (Scanning line: red line on the fusion zone; dash square: interface zone)

the heat input and the remelting times of C0.2 are considerably larger than those of C0.5, the deeper fusion zone, and consequently, more aluminum diffusion into the fusion zone are acceptable. On the other hand, the amount of aluminum at the surface of the fusion zone of Al0.2 reaches about 50 wt.%, which is much higher than that of the C0.2 sample. Since both Al0.2 and C0.2 are treated with the same laser conditions, the higher Al diffusion into the fusion zone is originated from the thermal properties of Al alloy (or Al composite). The weld pool of the C0.2 sample is cooler and has lower thermal diffusivity than that of the Al0.2 one (Fig. 3); hence, less Al diffusion takes place within the weld pool of the C0.2 sample. It is anticipated that BNi-2 particles in the Cx samples would react with the molten aluminum and intervene easy aluminum diffusion within the weld pool.

3.4 Analysis of interface zone

BSE−SEM microstructure of the interface zone in Al0.4 is shown in Fig. 8. The structure is routine and is reported by other studies [5,10]. Regardless of the interface layer shape, micro-cracks are nucleated and grown through it. Another observation is the presence of islands like B (Table 3) with the similar chemical composition to the fusion zone (Al0.4 in Table 3). Their appearance more likely shows that a part of high-density molten or semi-solid weld pool has detached and advanced through the molten aluminum.

The chemical compositions of the assigned point at the interface layer (A in Fig. 8) is presented in Table 3. To predict the possible types of the IMC at the Point A, it

is assumed that Cr and Ni are dissolved in the iron matrix as a solid solution. According to the Al−Fe(,Cr,Ni) phase diagram [28], Al$_3$Fe(Ni,Cr) is the most probable intermetallic compound [5, 6], in which XRD pattern from the interface layer (Fig. 9) also confirms this result. Regardless of the chemical composition of the phases, all grey color phases are prone to micro-crack, which is due to the presence of the brittle phases with a probably high mismatch between their thermal expansion coefficient and that of the surrounding matrix.
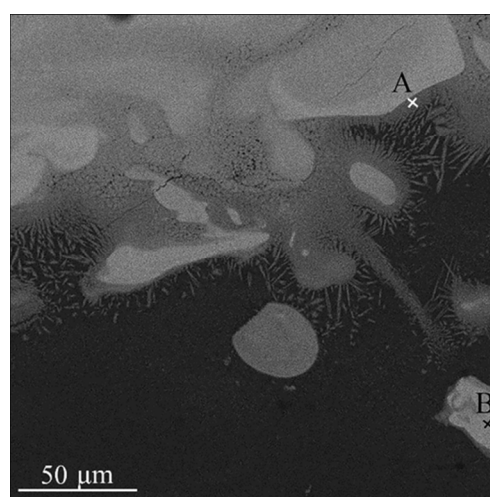

Fig. 8 BSE−SEM microstructure of Al0.4 sample at weld interface layer (Chemical compositions of assigned points are shown in Table 3)

Figure 10 depicts the interface zone of C0.3 sample. In contrast with Al0.4 interface (Fig. 8), there are new fine needle form reaction products placed a bit farther

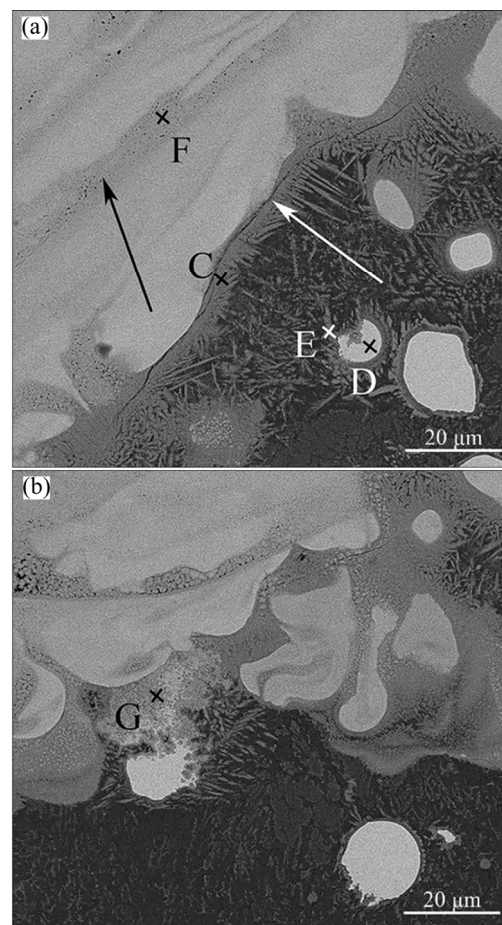**Table 3** Chemical compositions of points A−G in Figs. 8 and 10 (at.%)

Point	Al	Mg	Fe	Cr	Ni	Si	Possible aluminide phase
A	77.53	2.73	13.8	5.09	0.85	−	Al₃Fe(,Cr,Ni) [b]
B	53.8	2.31	32.46	10.83	2.92	−	Al₂Fe(,Cr,Ni)+Al−Fe(,Cr,Ni)
C	87.78	6.72	2.93	1.21	1.35	−	Al₃Fe(,Ni,Cr)
D	5.02	−	4.07	10.37	49.87	30.66	−
E	71.83	3.96	6.03	3.88	9.26	9.01	Al₃Ni(,Fe,Cr)
F	89.25	2.5	6.23	1.69	0.33	−	Al₃Fe(,Cr,Ni)
G	75.28	0.69	1.38	2.29	13.45	8.18	Al₃Ni(,Cr,Fe)
Al0.4 [a]	46.96	0.69	36.69	12.76	2.9		Al−Fe(,Cr,Ni)

a: The chemical composition of the fusion zone (black cursor in Fig. 5(c)); b: The elements in parentheses are considered as a solid solution. The order of elements iron, nickel and chromium is based on their contents
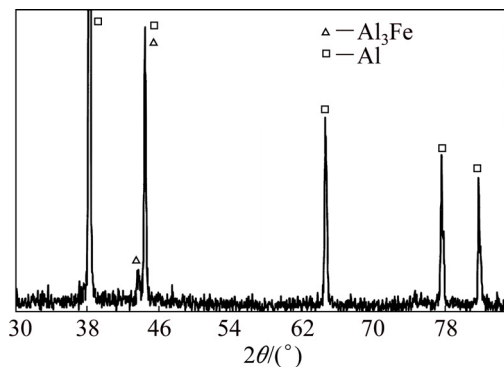

Fig. 9 XRD pattern from interface layer of Al0.4 sample

than the fusion zone border. The line scan of the distance between the fusion zone and the mention reaction products is shown in Fig. 11. As it can be seen, the fusion zone contains a mixture of Al and Fe(,Cr,Ni). By advancing into the Al composite base metal, the amounts of Fe and Cr reduce and the amount of Al increases. The reason would be the change of the base metal from DSS to the Al composite. However, the amount of the nickel is initially declined and then increased. Since the DSS contains about 5 wt.% nickel, the general fade of DSS by moving into the Al composite leads to the decline of Ni. After that, the BNi-2 particles would play an important role so that the amount of nickel becomes significantly higher than that of iron and chromium at the end of the line.

Point C in Fig. 10(a) corresponds to the Point A in Fig. 8, but with higher nickel content (Table 3). According to PIKE et al [29], the high content of Fe at the interface layer increases the chance of iron aluminide IMC formation, which can result in a brittle interface layer. On the other hand, the ratio of Fe/Ni decreases at Point C (Fig. 10), indicating that nickel was injected from both DSS plate and BNi-2 particles in the weld pool. It is expected that the presence of higher nickel at the interface of Cx samples, either as a solid solution or as a softer intermetallic compound, enhances the mechanical behavior of the interface (as will be discussed in Section 3.6).

Fig. 10 Microstructures of different parts of C0.3 samples in high magnifications (White arrows show micro-cracks, black arrow indicates dark bands, and the chemical composition of assigned points are shown in Table 3)

Another interaction at the interface could be the interaction between BNi-2 particles and surrounding Al matrix. Chemical composition of the Point D (Fig. 10(a) and Table 3) shows that some parts of the reinforced particle have still remained intact at the interface, while it gradually dissolves and reacts at its interface with the surrounding molten aluminum, as the chemical composition of Point E (Fig. 10(a)) in Table 3 indicates.
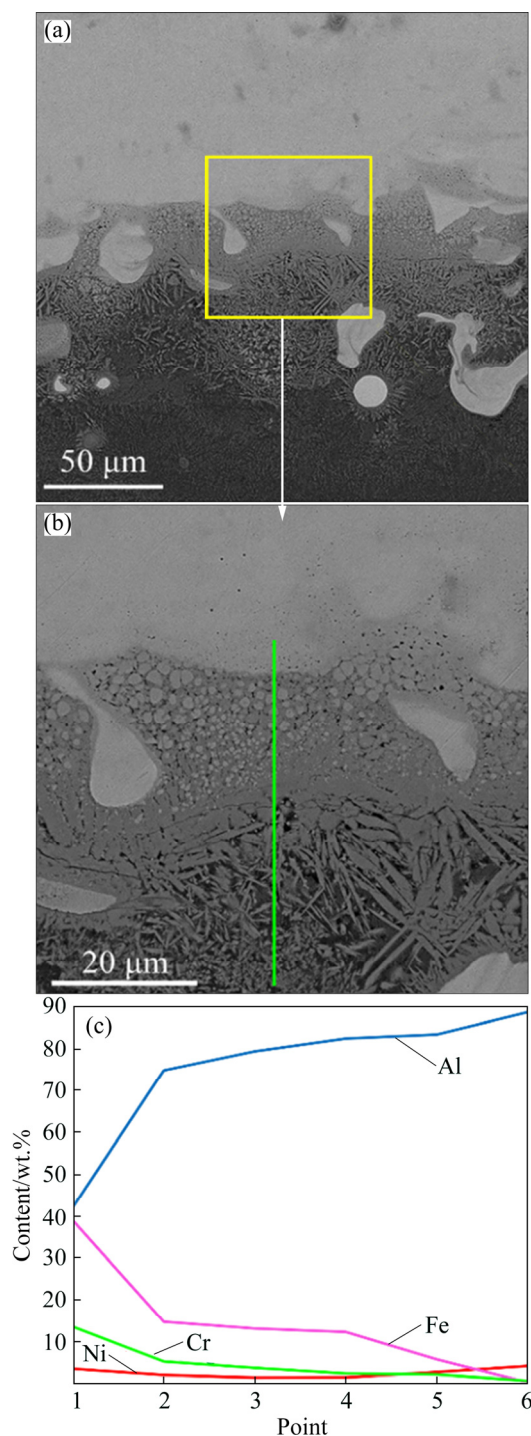
Fig. 11 Interface zone of C0.3 sample (a, b) and SEM line scan result (c) of interface

Point F presents the chemical composition of the dark bands (black arrow in Fig. 10). Such bands have less aluminum plus magnesium content compared to the point C.

All reaction products at the interface have needle form, which indicates the formation of IMC [6]. However, there would be another interaction when the cooled and solid weld metal is in contact with molten

BNi-2 and aluminum (e.g. Point G in Fig. 10(b)). The molten particle has low amount of Fe (Point G in Table 3) and is free from the IMC needles and also micro-cracks. The presence of such molten particles (Point G) can suppress the micro-crack growth at the interface.

3.5 Hardness

Hardness profiles of the fusion zones in various samples, at their centerlines from DSS top side towards aluminum downside (Fig. 2), are shown in Fig. 12. All samples almost follow a similar pattern in their hardness profiles. Three regions could be recognized. The first one is the fusion zone (DSS) region with almost constant hardness from its surface to the area close to the interface region. The second region is the interface region (a mixed area from DSS, interface layer and aluminum), in which its hardness increases to a maximum at the interface layer, and then almost drops to the hardness value of the aluminum alloy base metal, as the third region.
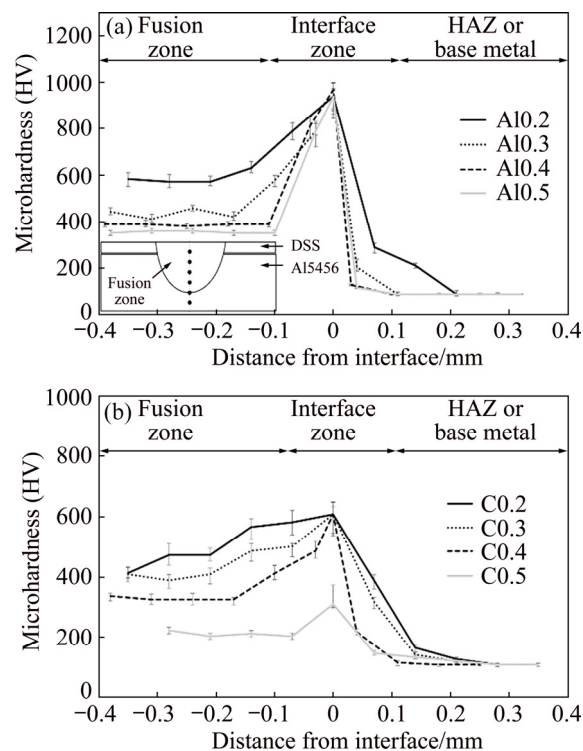
Fig. 12 Hardness profiles of fusion zones at their center lines: (a) Al*x* sample; (b) C*x* sample

The hardness profiles indicate that overall level of hardness increases with the decrease in the laser pulse distance. The reason would be higher heat energy input during shorter laser pulses intervals, which increases temperature and aluminum content of the weld pool (Figs. 3 and 7). The situation enhances the intermixing volume of DSS and aluminum in the weld pool. Therefore, proper conditions are promoted for the

precipitation of a greater amount of Al−Fe(,Cr,Ni) IMC. Higher molten pool penetration in Alx samples (Figs. 5 and 6(b)) demonstrates that aluminum content is higher in Alx samples rather than that in Cx samples. This means the proper conditions for higher precipitation of aluminides are prepared in Alx samples. Hence, the hardness levels of Alx samples are considerably higher, ranging 400−970 HV, while hardness levels in the Cx samples range from 220 to 600 HV.

The higher hardness of the DSS/aluminum interfaces of all Alx samples is due to the presence of IMC like Al$_3$Fe (Fig. 9) or Al$_5$Fe$_2$ and Al$_2$Fe [30], which increase the hardness up to 970 HV. The maximum hardness is remarkably lower in the Cx samples and ultimately achieves to ~600 HV. The difference between maximum hardness values in Alx and Cx samples is due to differences in the type of IMC at their interfaces, where IMCs at interfaces in the Alx samples are mainly iron aluminide compounds, but those contain more nickel and nickel-bearing compounds in the Cx samples (Table 3). According to PIKE et al [29], nickel significantly decreases the hardness of Fe−Al IMC. Among all samples, hardness of the interface layer in the C0.5 sample is quite low. It had the least temperature during welding process (Fig. 3), whereas minimum intermixing and reactions have expected at its interface.

3.6 Shear strength

All weldments, except C0.4 and C0.5 ones, contain cracks (Fig. 5), which definitely decrease the shear strengths of the samples. Nevertheless, they were examined under shear tests. The results (Fig. 13) show that shear strengths of the samples are low at short laser pulse distances, and increase by the pulse distance.
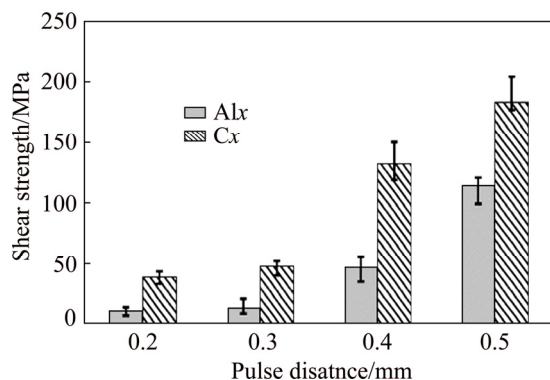

Fig. 13 Shear strength of rupture in different samples

Al0.2 and Al0.3 samples have the least strength, as they suffer from macro-cracks in their fusion zone (Fig. 5). Propagation of the macro-cracks and brittleness of the fusion zone in Al0.2 and Al0.3 samples are the reasons of easy rupture in these samples (Fig. 14).

By changing bottom-side metal base, from aluminum alloy to aluminum composite (i.e., from Al0.2 and Al0.3 to C0.2 and C0.3 samples), the rupture type changes from growing of macro-crack in the fusion zone to the propagation of micro-crack within the interface layer or the dark bands. Since the size of cracks becomes significantly smaller in C0.2 and C0.3 samples (Fig. 5), the required energy for crack growth would be greater, and the strength is over-tripled in comparison to the corresponding strengths in the Alx samples. This obviously clarifies that Ni-modified interface layers resist better against crack propagation. As a result, a wider range of the Al/DSS acceptable strength is achievable by reinforcing Al by BNi-2 particles. Observations on the rupture at higher magnification (Fig. 14(d)) reveal that the micro-cracks propagate through the dark bands. It is expected that the fusion zone around the interface demonstrates higher toughness and prevents micro-crack to grow within the fusion zone. Hence, the micro-cracks deviate at the interface and continue their path through the less-tough dark bands.

Longer pulse distance promotes the thinner interface layer and the lower amount of IMC in the weldment (Fig. 6(a)), whereas fracture toughness increases and better mechanical behavior has been prospected. Failure in the samples with long pulse distances (i.e., 0.4 and 0.5 mm) takes place via growing micro-cracks within the interface layer (Fig. 14), instead of the fusion zone. The thinner interface shows better resistance against micro-crack growth in comparison to the thicker one. The fracture toughness of thin layer would be higher as it would be in the plane stress regime; however, the toughness reduces via the increase in layer thickness [31].

In Al0.4 and Al0.5 samples, the Al0.5 has thinner interface layer (Fig. 6) and its strength should be higher [32]. Interestingly, by decreasing the interface layer from ~40 μm in Al0.4 to ~20 μm in Al0.5, the strength is increased by almost 1.5 folds, from 46 to 114 MPa. This clearly shows the beneficial effect of the thin interface on the shear strength.

Comparing Alx and Cx samples, at long pulse distances, reveals that C0.4 and C0.5 samples have the highest joint strengths. Such an improvement can be originated from the change at the interface characteristics. First, Cx samples have much thinner interface layer, ~15 and ~4 μm in C0.4 and C0.5, respectively (Fig. 6). Second, BNi-2 particles modify the interface zone by suppressing the crack growth, and also, reducing the hardness of the interface layer in the Cx samples than that of Alx samples (Fig. 12). As a consequence, weldment strengths in C0.4 and C0.5 samples are higher than those of Al0.4 and Al0.5 samples.

The increase in strength of C0.4 in comparison to Al0.4 is remarkable, whereas it triples, from 46 to
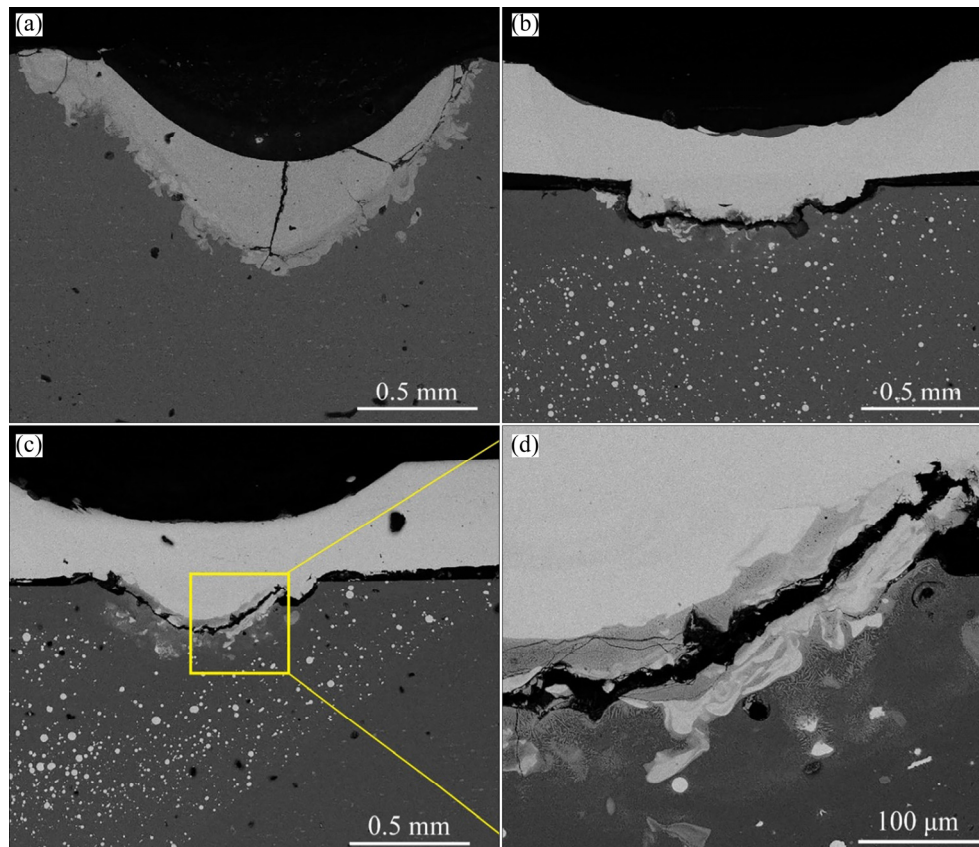
Fig. 14 Different types of ruptures in samples: (a) In fusion zone (samples Al0.2 and Al0.3); (b) At interface layer (samples Al0.4, Al0.5, C0.4 and C0.5); (c, d) Within dark bands (samples C0.2 and C0.3)

132 MPa. It is evidence that in addition to the Ni-modified interface layer, the thickness of the interface layer is halved in the C0.4 sample, in comparison to the Al0.4 sample.

The results show that the strength of the C0.5 sample is not so high, in comparison to that of Al0.5 and C0.4 samples, even though the C0.5 sample has the thinnest interface layer (Fig. 6) and no micro-crack is observed in its interface layer. This shows that other parameter(s) may encounter the final strength. TORKAMANY et al [5] explained that the intermix of two base metal is another important factor of concern. They suggested that, when intermix of the base metals is not complete, the joint strength reduces significantly, although the interface layer is thin. Accordingly, the C0.5 sample shows the least and incomplete intermixing at their interface, as it has experienced the least temperature (Fig. 3). Therefore, its strength is not as high as expected.

Thickness of the interface layer and height of the fusion zone (as a criterion of base metal intermixing) affect the final shear strength. The relationships are shown in Fig. 15 for both cases, aluminum alloy (Alx) and aluminum composite (Cx) as substrates. By surface fitting (Originlab pro v8.6 software), the following
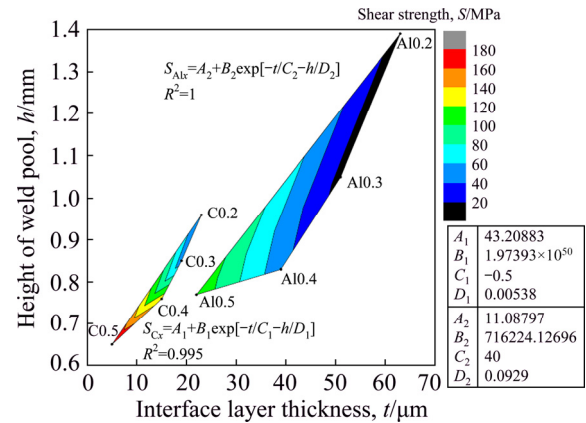
Fig. 15 shear strength versus interface thickness and height of weld pool (The color legend shows levels of shear strength; the fitting constants are shown at the side tables)

exponential relations are resulted for predicting the bonding strength:

For aluminum alloy base metal,

$$S_{Alx} = A_1 + B_1 \exp\left(-\frac{t}{c_1} - \frac{h}{D_1}\right), R^2 = 0.995 \qquad (5)$$

For aluminum composite base metal,

$$S_{Cx} = A_2 + B_2 \exp\left(-\frac{t}{c_2} - \frac{h}{D_2}\right), R^2 = 1 \qquad (6)$$

where S, t and h are the shear strength, the thickness of the interface layer and the weld pool height, respectively. The equation constants are also shown in Fig. 15. It should be mentioned that both the thickness of the interface layer and the height of the weld pool are the dependent variables of the pulse distance and the type of aluminum base metal (as shown in Fig. 6).

4 Conclusions

(1) Laser welding of 1.4362 DSS to Al5456 alloy was always encountered cracking at the interface layer or fusion zone.

(2) Cx samples have cooler weld pool and need more heat input for molten pool penetration.

(3) Laser welding of 1.4362 DSS to Al5456/BNi-2 composite provided a thinner interface layers, containing Ni-bearing IMC. Their interface was softer and less prone to crack, in comparison to the Alx ones.

(4) Higher laser pulse distances promoted less susceptibility to crack at weld metals.

(5) The Cx weldments tolerated higher shear forces before rupture.

(6) The Cx samples, with 0.4 and 0.5 mm laser pulse distances, were demonstrated the highest strength among all the samples.

References

[1]   SPRINGER H, KOSTKA A, PAYTON E J, RAABE D, KAYSSER-PYZALLA A, EGGELER G. On the formation and growth of intermetallic phases during interdiffusion between low-carbon steel and aluminum alloys [J]. Acta Materialia, 2011, 59(4): 1586−1600.

[2]   MECO S, COZZOLINO L, GANGULY S, WILLIAMS S, MCPHERSON N. Laser welding of steel to aluminium: Thermal modelling and joint strength analysis [J]. Journal of Materials Processing Technology, 2017, 247(Supplement C): 121−133.

[3]   QIU Ran-feng, IWAMOTO C, SATONAKA S. The influence of reaction layer on the strength of aluminum/steel joint welded by resistance spot welding [J]. Materials Characterization, 2009, 60(2): 156−159.

[4]   WANG Peng-fei, CHEN Xi-zhang, PAN Qiu-hong, MADIGAN B, LONG Jiang-qi. Laser welding dissimilar materials of aluminum to steel: An overview [J]. The International Journal of Advanced Manufacturing Technology, 2016, 87(9): 3081−3090.

[5]   TORKAMANY M J, TAHAMTAN S, SABBAGHZADEH J. Dissimilar welding of carbon steel to 5754 aluminum alloy by Nd:YAG pulsed laser [J]. Materials & Design, 2010, 31(1): 458−465.

[6]   SIERRA G, PEYRE P, DESCHAUX-BEAUME F, STUART D, FRAS G. Steel to aluminium key-hole laser welding [J]. Materials Science and Engineering A, 2007, 447(1): 197−208.

[7]   MATHIEU A, SHABADI R, DESCHAMPS A, SUERY M, MATTEÏ S, GREVEY D, CICALA E. Dissimilar material joining using laser (aluminum to steel using zinc-based filler wire) [J]. Optics & Laser Technology, 2007, 39(3): 652−661.

[8]   SIERRA G, PEYRE P, DESCHAUX BEAUME F, STUART D, FRAS G. Galvanised steel to aluminium joining by laser and GTAW processes [J]. Materials Characterization, 2008, 59(12): 1705−1715.

[9]   YANG Jin, LI Yu-long, ZHANG Hua, GUO Wei, WECKMAN D, ZHOU N. Dissimilar laser welding/brazing of 5754 aluminum alloy to DP 980 steel: Mechanical properties and interfacial microstructure [J]. Metallurgical and Materials Transactions A, 2015, 46(11): 5149−5157.

[10]   CHEN Shu-hai, HUANG Ji-hua, MA Ke, ZHAO Xing-ke, VIVEK A. Microstructures and mechanical properties of laser penetration welding joint with/without Ni-foil in an overlap steel-on-aluminum configuration [J]. Metallurgical and Materials Transactions A, 2014, 45(7): 3064−3073.

[11]   ZHANG Yi, LI Fu-nan, GUO Guan-lin, WANG Gang, WEI Hai-ying. Effects of different powders on the micro-gap laser welding-brazing of an aluminium-steel butt joint using a coaxial feeding method [J]. Materials & Design, 2016, 109: 10−18.

[12]   YU J, CHO S M. Metal-cored welding wire for minimizing weld porosity of zinc-coated steel [J]. Journal of Materials Processing Technology, 2017, 249: 350−357.

[13]   YANG Jin, LI Yu-long, ZHANG Hua. Microstructure and mechanical properties of pulsed laser welded Al/steel dissimilar joint [J]. Transactions of Nonferrous Metals Society of China, 2016, 26(4): 994−1002.

[14]   YADAV D, BAURI R. Processing, microstructure and mechanical properties of nickel particles embedded aluminium matrix composite [J]. Materials Science and Engineering A, 2011, 528(3): 1326−1333.

[15]   ESMAILY H, HABIBOLAHZADE A, AJALLY M. Parametric investigation of Al5456/BNi-2 composite properties fabricated by friction stir processing [J]. Journal of Alloys and Compounds, 2017, 725: 1044−1054.

[16]   SHANG S, WELLBURN D, SUN Y Z, WANG S Y, CHENG J, LIANG J, LIU C S. Laser beam profile modulation for microstructure control in laser cladding of an NiCrBSi alloy [J]. Surface and Coatings Technology, 2014, 248: 46−53.

[17]   HUANG W, CHANG Y A. Thermodynamic properties of the Ni−Al−Cr system [J]. Intermetallics, 1999, 7(8): 863−874.

[18]   JACOBS M H G, SCHMID-FETZER R, MARKUS T, MOTALOV V, BORCHARDT G, SPITZER K H. Thermodynamics and diffusion in ternary Fe−Al−Cr alloys. Part I: Thermodynamic modeling [J]. Intermetallics, 2008, 16(8): 995−1005.

[19]   CHRIFI-ALAOUI F Z, NASSIK M, MAHDOUK K, GACHON J C. Enthalpies of formation of the Al−Ni intermetallic compounds [J]. Journal of Alloys and Compounds, 2004, 364(1): 121−126.

[20]   GĄSIOR W, DĘBSKI A, MOSER Z. Formation enthalpy of intermetallic phases from Al−Fe system measured with solution calorimetric method [J]. Intermetallics, 2012, 24: 99−105.

[21]   ASM Handbook, Volume 02: Properties & selection: Nonferrous alloys and special-purpose materials [M]. Materials Park, OH: ASM International, 1990.

[22]   PAL R. On the Lewis–Nielsen model for thermal/electrical conductivity of composites [J]. Composites Part A: Applied Science and Manufacturing, 2008, 39(5): 718−726.

[23]   MARCOS-GÓMEZ D, CHING-LLOYD J, ELIZALDE M R, CLEGG W J, MOLINA-ALDAREGUIA J M. Predicting the thermal conductivity of composite materials with imperfect interfaces [J]. Composites Science and Technology, 2010, 70(16): 2276−2283.

[24]   HSU H C, YEH C T, TUAN W H. Heat capacity of Al$_2$O$_3$-NiAl composites, a key parameter for thermal management [J]. Ceramics International, 2017, 43(Supplement 1): S705−S709.

[25]   FUKUI Y, OKADA H, KUMAZAWA N, WATANABE Y, YAMANAKA N, OYA-SEIMIYA Y. Manufacturing of Al−Al$_3$Fe functionally graded material using the vacuum centrifugal method and measurements of its mechanical properties [J]. Journal of Japan Institute of Light Metals, 1999, 49(1): 35−40.

[26]   BELOV N A, AKSENOV A A, ESKIN D G. Iron in aluminium alloys: Impurity and alloying element [C]. FRIDLYANDER J N, ESKIN D

G. Advances in Metallic Alloys. London: Taylor & Francis, 2002.

[27] KATAYAMA S, KOBAYASHI Y, MIZUTANI M, MATSUNAWA A. Effect of vacuum on penetration and defects in laser welding [J]. Journal of Laser Applications, 2001, 13(5): 187−192.

[28] PAVLYUCHKOV D, PRZEPIÓRZYŃSKI B, KOWALSKI W, VELIKANOVA T Ya, GRUSHKO B. Al−Cr−Fe phase diagram: Isothermal sections in the region above 50 at% Al [J]. Calphad, 2014, 45(Supplement C): 194−203.

[29] PIKE L M, ANDERSON I M, LIU C T, CHANG Y A. Site occupancies, point defect concentrations, and solid solution hardening in B2 (Ni,Fe)Al [J]. Acta Materialia, 2002, 50(15):

3859−3879.

[30] LEE K J, KUMAI S. Characterization of intermetallic compound layer formed at the weld interface of the defocused laser welded low carbon steel/6111 aluminum alloy lap joint [J]. Materials Transactions, 2006, 47(4): 1178−1185.

[31] ASKELAND D R, FULAY P P, WRIGHT W J. The science and engineering of materials [M]. USA: CL-Engineering, 2011.

[32] SHAHVERDI H R, GHOMASHCHI M R, SHABESTARI S, HEJAZI J. Microstructural analysis of interfacial reaction between molten aluminium and solid iron [J]. Journal of Materials Processing Technology, 2002, 124(3): 345−352.

采用 BNi-2 钎焊合金和搅拌摩擦加工提高双向不锈钢与铝合金的脉冲激光焊接性能

Hossein ESMAILY, Ali HABIBOLAHZADEH, Mohammad TAJALLY

Faculty of Materials and Metallurgical Engineering, Semnan University, Semnan 35351-19111, Iran

摘　要：研究激光脉冲距离和 5456 铝合金强化对其与双相不锈钢 (DSS) 板激光焊接性能的影响。首先，采用镍基 BNi-2 钎焊粉通过搅拌摩擦加工增强铝合金板；然后，将 DSS 板分别与 Al5456 铝合金板和 Al5456/BNi-2 复合材料进行激光焊接。采用扫描电镜、X 射线衍射仪、显微硬度仪和剪切试验等方法对焊接区进行研究。结果显示，随着激光脉冲距离从 0.2 mm 增加到 0.5 mm，焊接界面层从 23 μm 减小到 5 μm。由于铝合金的增强相 BNi-2 向熔池中注入更多的镍，导致界面层的析出相由 DSS/铝合金焊缝中的 Al−Fe 金属间化合物(IMCs) 转变为 DSS/Al 复合材料焊缝中的 Al−Ni−Fe 金属间化合物(IMCs)，因此，焊缝裂纹倾向显著降低，界面层硬度由~950 HV 降低到~600 HV。与 DSS/Al 焊缝相比，DSS/Al 复合材料焊缝的剪切强度提高~150%，从 46 MPa 提高到 114 MPa。

关键词：双相不锈钢(DSS)；Al5456 铝合金；BNi-2 钎焊合金；搅拌摩擦加工；脉冲激光焊接

(Edited by Bing YANG)